Balanced Contribution to the Intensification of a Tropical Cyclone Simulated in TCM4: Outer-Core Spinup Process*

HIRONORI FUDEYASU[+] AND YUQING WANG

*International Pacific Research Center, School of Ocean and Earth Science and Technology,
University of Hawaii at Manoa, Honolulu, Hawaii*

ABSTRACT

The balanced contribution to the intensification of a tropical cyclone simulated in the three-dimensional, nonhydrostatic, full-physics tropical cyclone model version 4 (TCM4), in particular the spinup of the outer-core circulation, is investigated by solving the Sawyer–Eliassen equation and by computing terms in the azimuthal-mean tangential wind tendency equation. Results demonstrate that the azimuthal-mean secondary circulation (radial and vertical circulation) and the spinup of the midtropospheric outer-core circulation in the simulated tropical cyclone are well captured by balance dynamics. The midtropospheric inflow develops in response to diabatic heating in mid–upper-tropospheric stratiform (anvil) clouds outside the eyewall in active spiral rainbands and transports absolute angular momentum inward to spin up the outer-core circulation. Although the azimuthal-mean diabatic heating rate in the eyewall is the largest, its contribution to radial winds and thus the spinup of outer-core circulation in the middle troposphere is rather weak. This is because the high inertial stability in the inner-core region resists the radial inflow in the middle troposphere, limiting the inward transport of absolute angular momentum. The result thus suggests that diabatic heating in spiral rainbands is the key to the continued growth of the storm-scale circulation.

1. Introduction

To first order, the primary circulation of a strong tropical cyclone can be considered as a warm-cored, quasi-axisymmetric vortex in gradient wind and hydrostatic balance. As a tropical cyclone evolves slowly while its primary circulation remains in gradient wind and hydrostatic balance, the secondary circulation (radial and vertical circulation) can be considered as a result of the response to both diabatic heating and momentum forcing, including surface friction. The secondary circulation transports high absolute angular momentum inward to spin up the tropical cyclone primary circulation. This spinup process can be well described by the Sawyer–Eliassen (SE) equation following the classic work of Eliassen (1952).

The general form of the SE equation is a two-dimensional diagnostic equation describing the azimuthal-mean secondary circulation forced by 1) axisymmetric diabatic heating, 2) eddy heat flux, 3) axisymmetric surface friction and subgrid-scale vertical mixing (frictional forcing), and 4) eddy momentum flux. Many theoretical studies have applied the SE equation to calculate the secondary circulation in response to idealized forcing mechanisms, such as point sources of diabatic heating and frictional forcing, excluding eddy heat and momentum fluxes (e.g., Willoughby 1979; Shapiro and Willoughby 1982; Schubert and Hack 1982; Holland and Merrill 1984; Hack and Schubert 1986; Pendergrass and Willoughby 2009). In these studies, diabatic heating is generally assumed to occur in a convective ring of the eyewall (EW) and is given as a prescribed function of radius and height (e.g., Pendergrass and Willoughby 2009). The solution of the SE equation in response to prescribed axisymmetric eyewall-like heating produces an updraft through the locus of heat source with the lower-tropospheric inflow and upper-tropospheric outflow, consistent with the axisymmetric conceptual model of a tropical cyclone.

Many aspects of a tropical cyclone can be explained based on the SE equation or often alternatively termed balance dynamics. In particular, contribution by balance dynamics to the intensification of a tropical cyclone has long been studied as a basic aspect of tropical cyclone dynamics in not only theoretical studies but also diagnostic studies from observations (e.g., Molinari and Vollaro 1990; Molinari et al. 1993) and full or simplified-physics model simulations (e.g., Persing et al. 2002; Möller and Shapiro 2002; Hendricks et al. 2004; Montgomery et al. 2006; Bui et al. 2009).

Persing et al. (2002) and Möller and Shapiro (2002) diagnosed the secondary circulation using the SE equation and discussed the intensity change of Hurricane Opal (1995). They showed that, with all forcing terms derived from the full-physics model output, the SE equation solution captured the model secondary circulation quite well. Möller and Shapiro (2002) found that, although contributions by diabatic heating and frictional forcing to tropical cyclone intensification were much greater, the eddy processes also contributed to the rapid intensification of Hurricane Opal to some degree. Hendricks et al. (2004) and Montgomery et al. (2006) demonstrated that the secondary circulation during the tropical cyclone genesis stage in a cloud-resolving model simulation could be well explained by balance dynamics in the context of the SE equation. Bui et al. (2009) investigated the extent to which the secondary circulation and intensification of a simulated tropical cyclone can be explained by balance dynamics. Their results further confirmed that the solution of the SE equation with all forcings from a simplified-physics model simulation well captured the secondary circulation of a simulated tropical cyclone, except in the boundary layer, where the unbalanced flow becomes significant. They also showed that inflow above the boundary layer in response to diabatic heating transports absolute angular momentum inward, spinning up the primary circulation in regions more than 150-km radius or in the outer-core region (between radii 1° and 2.5° latitude) as defined by Weatherford and Gray (1988a,b). This result thus demonstrated that, in addition to the storm intensity, the intensification of the primary circulation in the outer-core region can also be explained by balance dynamics.

Pendergrass and Willoughby (2009) found that the balanced response of the secondary circulation is sensitive to the radial location of heat source and the inertial stability of the vortex itself. In the inertially stable regions, the secondary circulation is confined horizontally close to the heat source. Because the inertial stability is generally high in the eyewall region, diabatic heating in the eyewall is expected to force relatively weak midtropospheric inflow in the inner-core region, contributing little to the

spinup of the outer-core circulation. This suggests that diabatic heating in the eyewall region enhanced the primary circulation mainly in the inner-core region and thus the storm intensity, whereas heat sources outside the eyewall could contribute the changes in primary circulation in the outer-core region and thus the size of a tropical cyclone. This indeed has been studied based on sensitivity experiments in idealized numerical simulations by Wang (2009), Hill and Lackmann (2009), and Xu and Wang (2010a). These studies show that diabatic heating in both inner and outer spiral rainbands contributes to the size increase of tropical cyclones. Therefore, diabatic heating outside the eyewall may contribute significantly to the intensification of the primary circulation in the outer-core region, where the inertial stability is much weaker than that in the eyewall. Although Bui et al. (2009) demonstrated the importance of diabatic heating to the spinup of the outer-core circulation above the inflow boundary layer they did not evaluate the relative contributions by heat source in different regions in their simulated storm.

The objective of this study is to extend Bui et al.'s (2009) work to examine forcings to the spinup of the outer-core primary circulation of a simulated tropical cyclone in a full-physics model under idealized conditions by solving the SE equation and by computing terms in the azimuthal-mean tangential wind equation. The SE equation is a linear partial differential equation and thus, for suitable boundary conditions, solutions to different forcings are additive. This allows us to evaluate contribution of heat source in different regions to the spinup of the outer-core circulation of the simulated tropical cyclone. The rest of the paper is organized as follows: the next section briefly describes the tropical cyclone model version 4 (TCM4) experiment and the SE equation. Section 3 validates the SE equation as a tool to diagnose the secondary circulation in the simulated tropical cyclone. Contributions of different forcing mechanisms to the spinup of the outer-core circulation in the simulated tropical cyclone are evaluated based on the azimuthal-mean tangential wind tendency equation in section 4. The main findings are summarized and discussed in the last section.

2. Methodology

a. TCM4 experiment

TCM4 is a fully compressible, quadruply nested, non-hydrostatic tropical cyclone model. The model physics include an E–ε turbulence closure scheme for subgrid-scale vertical turbulent mixing (Langland and Liou 1996); a modified Monin–Obukhov scheme for the surface flux calculation (Fairall et al. 2003); explicit treatment of mixed-phase cloud microphysics (Wang 2001); fourth-order horizontal diffusion with deformation-dependent

diffusion coefficient for all prognostic variables, except for that related to the mass conservation equation; a Newtonian cooling term added to the potential temperature equation to mimic radiative cooling as used in Rotunno and Emanuel (1987); and dissipative heating due to molecular friction, which is included by adding the turbulent kinetic energy dissipation rate ε into the thermodynamic equation. Because no large-scale environmental flow is included in this study, convection is mainly active within about a radius of 300 km from the storm center and thus is covered by the finest innermost domain. Therefore, cumulus parameterization is not used in this study. A complete description of TCM4 and its recent applications to the studies of tropical cyclone inner-core dynamics can be found in Wang (2007, 2008a,b, 2009), Wang and Xu (2010), and Xu and Wang (2010a,b).

The model has 32 vertical levels with relatively high resolution both in the lower troposphere and near the tropopause, and it has its lower boundary at a flat surface with the unperturbed surface pressure of 1010 hPa and its top at about 38 km. The four meshes are quadruply nested with two-way interactive nesting and with the inner meshes automatically moving to follow the model storm (Wang 2001, 2002). The outermost mesh has 251×251 grid points with a horizontal resolution of 67.5 km. The three inner meshes have 109×109, 127×127, and 271×271 grid points with horizontal resolutions of 22.5, 7.5, and 2.5 km, respectively.

Following the experimental design of Wang (2008a,b), the model was initialized with an axisymmetric cyclonic vortex in a quiescent environment over the ocean with a constant SST of 29°C and was run on an f plane of 18°N. The initial thermodynamic structure of the unperturbed model atmosphere is defined as the western Pacific clear-sky environment given in Gray et al. (1975). The initial cyclonic vortex has a maximum tangential wind speed of 20 m s^{-1} at the surface and at a radius of 80 km and decreases sinusoidally with pressure to vanish at 100 hPa. The mass and thermodynamic fields are obtained by solving the nonlinear balance equation as described in Wang (2001). Because our focus is on the detail structure of the developed tropical cyclone, the results in the innermost mesh with 15-min intervals after the 20-h spin-up period are used in the diagnostic and analyses discussed below. Thus, the TCM4 output with high temporal and spatial simulations allows us to study contributions to the intensification of the storm-scale circulation by heating source in different regions in the simulated storm.

b. The Sawyer–Eliassen equation

With the Boussinesq approximation, the SE equation in the radius–pseudoheight (r–Z) coordinates (Hendricks et al. 2004; Montgomery et al. 2006) can be written as

$$\frac{\partial}{\partial r}\left(\frac{A}{r}\frac{\partial\overline{\psi}}{\partial r} + \frac{B}{r}\frac{\partial\overline{\psi}}{\partial Z}\right) + \frac{\partial}{\partial Z}\left(\frac{C}{r}\frac{\partial\overline{\psi}}{\partial Z} + \frac{B}{r}\frac{\partial\overline{\psi}}{\partial r}\right)$$
$$= -\frac{\partial(\overline{\xi F})}{\partial Z} + \frac{\partial\overline{Q}}{\partial r}, \tag{1}$$

where r is radius, $\overline{\psi}$ is the azimuthal-mean transverse streamfunction explained by $\overline{v}_r = -(1/r)(\partial\overline{\psi}/\partial Z)$, $\overline{w} = (1/r)(\partial\overline{\psi}/\partial r)$, $\overline{v}_r$ is the azimuthal-mean radial wind, and $\overline{w}$ is the azimuthal-mean vertical velocity. The term Z is the pseudoheight defined as $Z = [1 - (p/p_0)^{R_d/C_p}](C_p\theta_0/g)$, where p is pressure, p_0 is a reference pressure (1000 hPa), R_d is the gas constant for dry air, C_p is the specific heat of dry air at constant pressure, g is the acceleration due to gravity, and θ_0 is a reference potential temperature (300 K). The overbar denotes the azimuthal mean at a constant pseudoheight about the circulation center. The left-hand side of Eq. (1) includes three parameters defined as

$$A = \overline{N^2} = \frac{g}{\theta_0}\frac{\partial\overline{\theta}}{\partial Z}, \text{ static stability;} \tag{2}$$

$$B = -\overline{\xi}\frac{\partial\overline{v}_t}{\partial Z}, \text{ baroclinicity; and} \tag{3}$$

$$C = \overline{\xi}\overline{\eta}, \text{ inertial stability,} \tag{4}$$

where $\overline{v}_t$ is the azimuthal-mean tangential wind, $\overline{\theta}$ is the azimuthal-mean potential temperature, $\overline{\eta} = f_0 + \overline{\zeta}$ is the azimuthal-mean absolute vertical vorticity, $\overline{\zeta}$ is the azimuthal-mean relative vertical vorticity, f_0 is the planetary vorticity at the cyclone center (18°N), and $\overline{\xi} = f_0 + 2\overline{v}_t/r$ is the vortex inertial parameter of the swirling flow. Terms on the right-hand side of Eq. (1) are those due to heat source and momentum forcing,

$$\overline{Q} = \frac{g}{\theta_0}\left(-\overline{v'_r\frac{\partial\theta'}{\partial r}} - \overline{w'\frac{\partial\theta'}{\partial Z}} + \dot{\overline{\theta}}\right), \text{ heating source, and} \tag{5}$$

$$\overline{F} = -\overline{v'_r\zeta'} - \overline{w'\frac{\partial v'_t}{\partial Z}} + \overline{F}_{sg}, \text{ momentum forcing,} \tag{6}$$

where the prime denotes the deviation (eddy) from the azimuthal mean. In Eq. (5), the first two terms represent the azimuthal-mean eddy radial and vertical fluxes of the asymmetric potential temperature and $\dot{\overline{\theta}}$ is the azimuthal-mean diabatic heating rate. Terms in Eq. (6) represent the azimuthal-mean eddy radial and vertical fluxes of the asymmetric tangential wind and the azimuthal-mean frictional forcing $\overline{F}_{sg}$, including subgrid-scale vertical turbulent mixing and surface friction. TCM4 provides a complete dynamically consistent dataset, including diabatic heating $\dot{\overline{\theta}}$ and friction $\overline{F}_{sg}$ with high temporal and spatial resolutions.

Given the structure of the vortex, thus the parameters A, B, and C defined in Eqs. (2)–(4) and the distribution of heating source and momentum forcing in Eqs. (5) and (6), the solution of Eq. (1) will give the secondary circulation if the elliptical discriminant condition $A \cdot C - B^2 > 0$ is satisfied everywhere in the vortex and proper boundary conditions are specified (Shapiro and Willoughby 1982). Although the discriminant derived from TCM4 output is positive throughout the middle–lower troposphere, there are small negative values in the upper-tropospheric outflow (see Fig. 4a), similar to those in Hendricks et al. (2004). In our calculations, if the absolute vorticity $\overline{\eta} = f_0 + \zeta < 0.5 \times f_0$, we set $\overline{\eta} = 0.5 \times f_0$ to allow the discriminant to be satisfied. This does not affect the global solution to the SE equation as we tested (Fudeyasu et al. 2010). The boundary conditions for the SE equation are $\overline{\Psi} = 0$ at $r = 0$ km, $Z = 0$ km, and Z_{top} and $\partial \overline{\Psi}/\partial r = 0$ as $r = \infty$, where Z_{top} is the top of the computational domain, which is 0–18 km in the vertical with 500-m grid interval and 0–300 km in the radial direction with 2.5-km grid spacing. To match the SE equation calculation, all fields of TCM4 output are first interpolated into the radius–pseudoheight coordinates.

3. Diagnostics of the secondary circulation

Figure 1 shows the time–radius cross section of the azimuthal-mean tangential wind averaged in the middle troposphere between 3- and 9-km heights. The simulated tropical cyclone intensified rapidly until 48 h with the maximum azimuthal-mean tangential wind increased to about 50 m s^{-1} and the radius of maximum wind decreased to about 30 km. This intensification was followed by a quasi-steady evolution. In the outer-core region,[1] the azimuthal-mean tangential wind strengthened intermittently in the simulation, implying a corresponding increase in the storm-scale size. Three episodes of the increase in the outer-core azimuthal-mean tangential wind occurred during 32–48, 56–78, and 86–96 h, respectively, corresponding to the episodes of active spiral rainbands as will be discussed later. This indicates that the spinup of the outer-core circulation in the middle troposphere could be closely related to the activity of spiral rainbands in the simulated storm.

Figure 2 shows the surface rain rate, its azimuthal mean, the east–west cross section of radar reflectivity across the

---

[1] Here we define the inner core as the region including the eye, eyewall, and inner rainbands within about a 70-km radius, whereas the outer core is defined as the region immediately outside the inner-core region including the outer rainbands and the associated anvil clouds in the outflow layer in the upper troposphere between radii of 70 and 210 km.
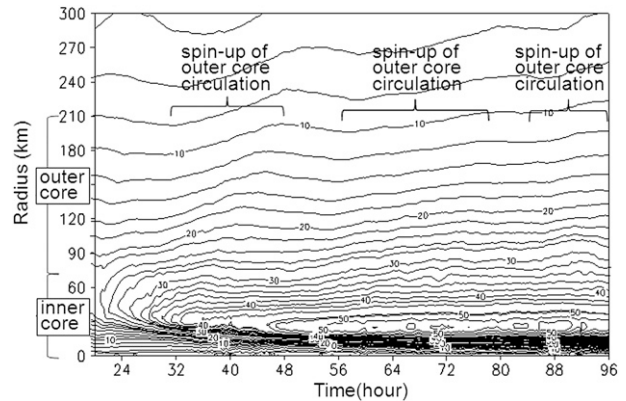
FIG. 1. Time–radius cross section of the azimuthal-mean tangential wind (m s^{-1}) averaged between 3- and 9-km heights. Contour interval is 2 m s^{-1}.

tropical cyclone center, and the azimuthal-mean radar reflectivity, all averaged between 71 and 72 h of simulation, during which the storm-scale size increased (Fig. 1). The surface rainfall field (Fig. 2a) displays a quasi-axisymmetric pattern in the inner-core region and shows little rainfall in the eye, which is surrounded by a closed heavy rainfall ring in the eyewall between radii of 15 and 30 km. Immediately outside the eyewall are the well-organized fine inner spiral rainbands, mainly within a radius of around 70 km. Outside the inner core, convection is loosely organized in two major outer spiral rainbands. The azimuthal-mean rainfall rate shows two peaks (Fig. 2b): one over 80 mm h^{-1}, at about 20-km radius in the eyewall, and the other at about 40 mm h^{-1}, near the 40-km radius associated with inner rainbands (IB).

The eyewall is characterized by high reflectivity throughout the troposphere (Fig. 2c). The weak reflectivity in the eye indicates the existence of hub clouds, and the high reflectivity immediately outside the eyewall is associated with inner spiral rainbands. The relatively high reflectivity between radii of 90 and 110 km to the west of the storm center is associated with an outer rainband (OB; Fig. 2a). Weak reflectivity in the middle–upper troposphere extending radially outward up to a radius of 180 km indicates the existence of anvil (stratiform) clouds in the outflow layer. The azimuthal-mean radar reflectivity shows high reflectivity in the eyewall and inner rainband and relatively weak reflectivity in the outer rainband and anvil clouds (Fig. 2d), consistent with observations (e.g., Barnes et al. 1983; Marks and Houze 1987; Marks et al. 2008).

The axisymmetric structure and some other dynamical parameters of the simulated storm averaged between 71 and 72 h are shown in Figs. 3 and 4. The storm develops a strong inflow in the boundary layer, an outflow in the
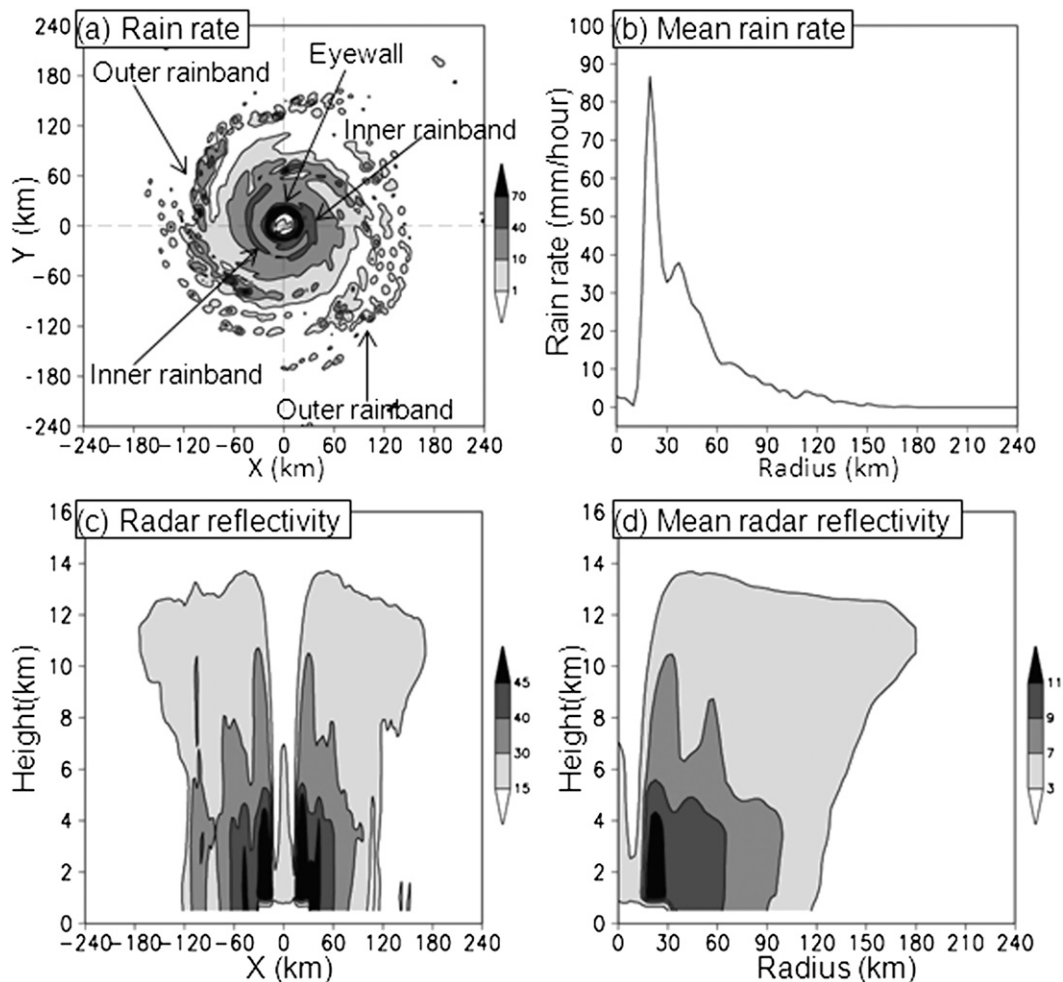
FIG. 2. (a) Plane view of rain rate (mm h^{-1}), (b) radial distribution of the azimuthal-mean rain rate (mm h^{-1}), (c) vertical (pseudoheight) cross section of radar reflectivity (dBZ) along the east–west direction across the storm center, and (d) the azimuthal-mean radar reflectivity (dBZ), all hourly averaged between 71 and 72 h of simulation. Regions with rain rate greater than 1 mm h^{-1} are shaded in (a). Regions with radar reflectivity higher than 15 and 3 dBZ are heavily and lightly shaded in (c) and (d), respectively.

upper troposphere (Fig. 3a), strong updrafts in the eyewall and inner rainband, and descent in the eye (Fig. 3b). In addition to the inflow in the boundary layer, a relatively weak inflow occurs outside the eyewall in the middle troposphere between 3- and 9-km heights (Fig. 3a). Tangential winds show the maximum over 70 m s^{-1}, just above the surface at a radius of about 20 km under the eyewall (Fig. 3c), The storm has a warm core in the middle–upper troposphere with the maximum temperature anomaly over 18 K (Fig. 3d). The absolute vertical vorticity shows an off-center maximum inside the eyewall throughout the troposphere (Fig. 4a). The surface of absolute angular momentum defined as $\overline{\Lambda} = r\overline{v}_t + f_0(r^2/2)$ is upright in the eyewall in the middle–lower troposphere but tilts outward with height in the upper troposphere and outside the eyewall (Fig. 4b). The inertial stability

parameter is high in the inner-core region (larger than 1×10^{-6} s^{-2}) but decreases rapidly outward and becomes less than 1×10^{-8} s^{-2} outside a radius of 60 km in the outer-core region (Fig. 4c).

Because the SE equation is based on the assumption of gradient wind balance, it is necessary to see to what extent the simulated tropical cyclone remains in the quasi-balanced state. Figure 4d shows the radial–height distribution of agradient tangential winds, defined as $\overline{v}_a = \overline{v}_t - \overline{v}_g$, where $\overline{v}_g$ is gradient wind calculated from the azimuthal-mean perturbation pressure field in TCM4. Positive agradient winds, namely supergradient winds, appear in the boundary layer under the eyewall because of surface friction, consistent with previous studies (e.g., Kepert and Wang 2001; Smith and Montgomery 2008; Smith et al. 2009). Relatively large positive and negative
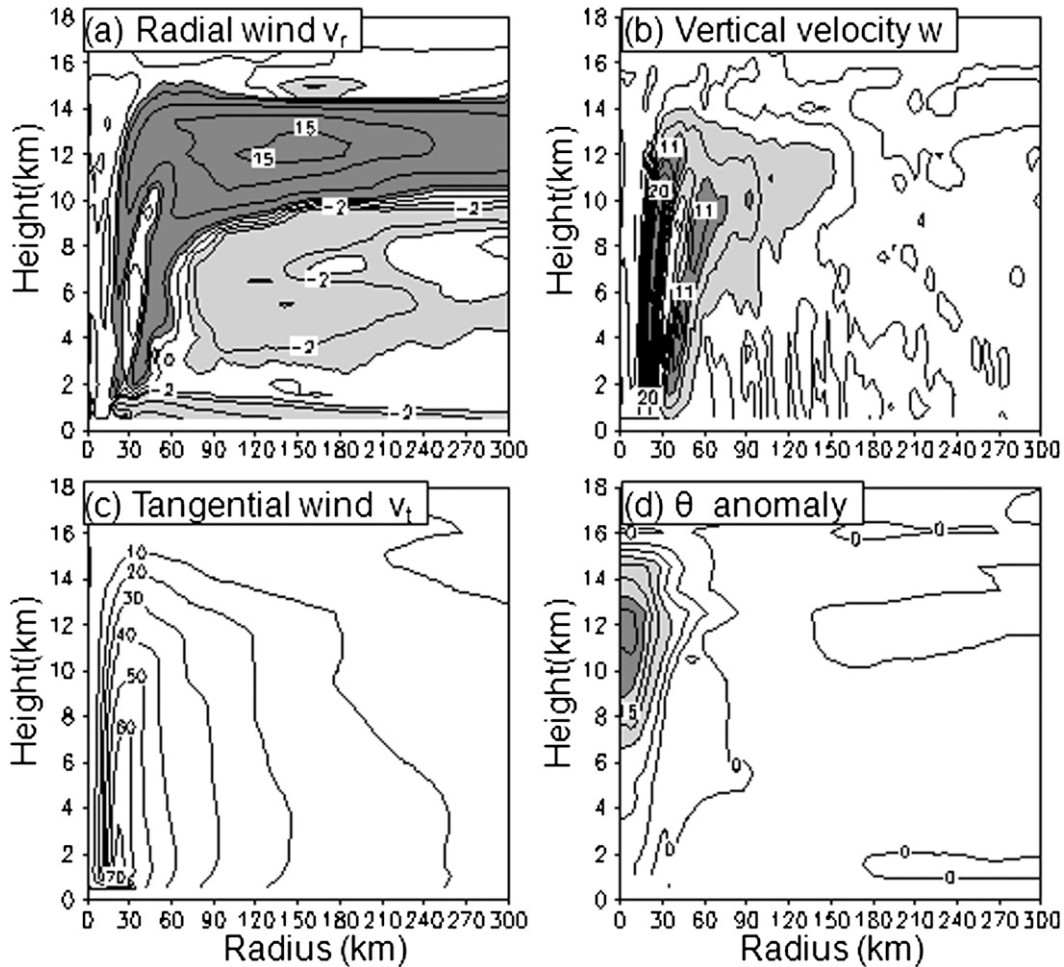
FIG. 3. The vertical structure of the simulated storm in pseudoheight coordinates. The azimuthal-mean (a) radial wind ($m\ s^{-1}$), (b) vertical velocity ($10^{-1}\ m\ s^{-1}$), (c) tangential wind ($m\ s^{-1}$), and (d) temperature anomaly (K), all averaged between 71 and 72 h of simulation. Contours are at 0 (thick), ± 1, ± 2, ± 5, ± 10, and $\pm 15\ m\ s^{-1}$, and regions with values greater than $1\ m\ s^{-1}$ (less than $-1\ m\ s^{-1}$) are heavily (lightly) shaded in (a). Contours are at 0 (thick), ± 2, ± 5, ± 8, ± 11, ± 14, ± 17, ± 20, and $\pm 23 \times 10^{-1}\ m\ s^{-1}$, and regions with values larger than $2 \times 10^{-1}\ m\ s^{-1}$ ($8 \times 10^{-1}\ m\ s^{-1}$) are lightly (heavily) shaded in (b). Contour interval is $10\ m\ s^{-1}$ in (c). Contour interval is 3 K, and regions with values larger than 9 K (18 K) are lightly (heavily) shaded in (d).

agradient winds occur in the upper-tropospheric outflow layer mainly because of the eddy effects, similar to those shown in Möller and Shapiro (2002). The agradient winds are overall small compared with the gradient winds, in particular in the middle troposphere below 10-km height above the inflow boundary layer, consistent with Bui et al. (2009). Therefore, the SE equation is applicable for the purpose of this study.

Figures 5a,b show the radial wind and vertical velocity obtained from the SE equation with all forcing terms in Eqs. (5) and (6). The SE equation solution captures the secondary circulation simulated in TCM4 well (Figs. 3a,b). To validate quantitatively, we show in Figs. 5c,d the normalized differences between the radial wind and

vertical velocity derived from the SE equation and those from TCM4, defined as $D = |SE - TCM4|/|TCM4|$. Note that regions with radial wind less than $1\ m\ s^{-1}$ and vertical velocity less than $0.2\ m\ s^{-1}$ in TCM4 are not shown in Figs. 5c,d. The D values in vertical velocity are small (less than 0.2) in the inner-core region, and those in radial wind are small (less than 0.3), except in the boundary layer and in the upper-tropospheric outflow layer. The D values larger than 0.4 are shown in regions where relatively strong agradient winds occur (Fig. 4d). Therefore, the azimuthal-mean secondary circulation simulated in TCM4 can be well explained by balance dynamics, in particular in the middle–lower troposphere, except in the boundary layer.
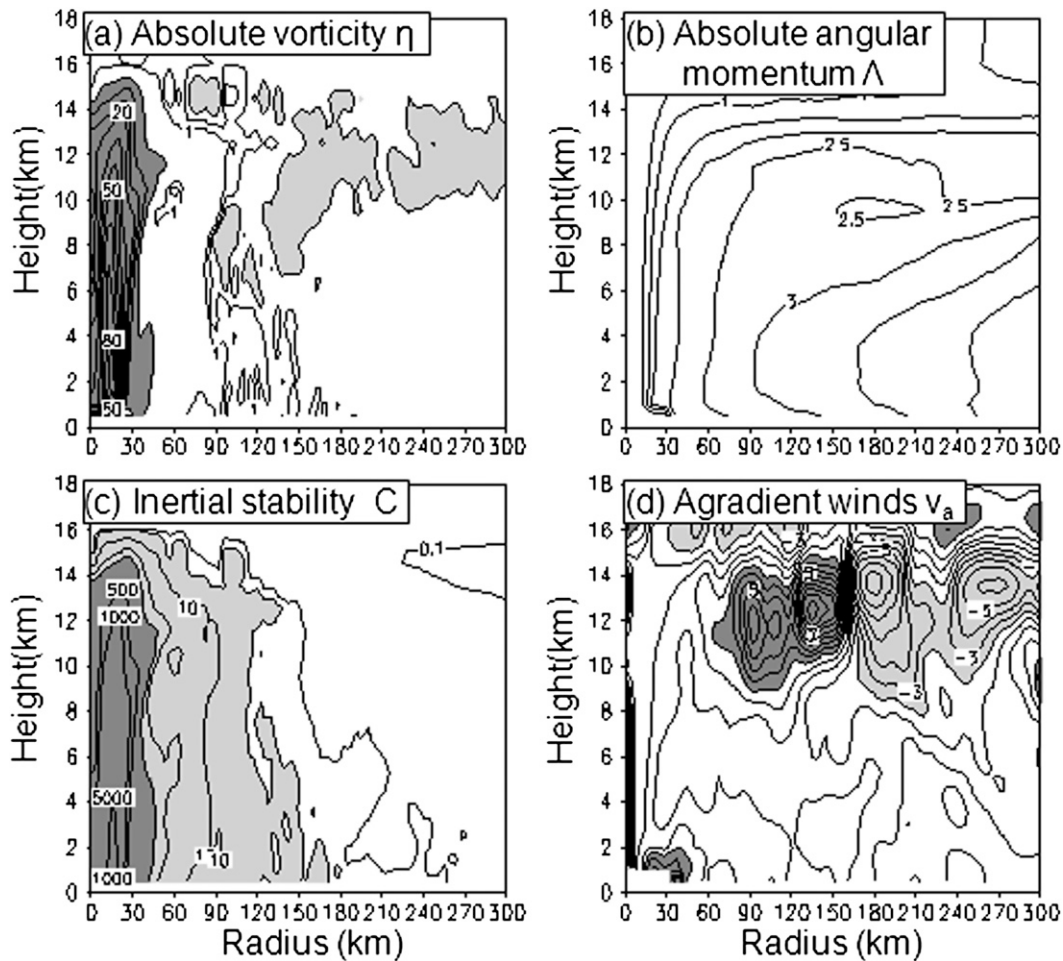
FIG. 4. The vertical cross section of the azimuthal-mean (a) absolute vertical vorticity (10^{-4} s^{-1}), (b) absolute angular momentum (10^6 m^2 s^{-1}), (c) inertial stability (10^{-8} s^{-2}), and (d) agradient winds (m s^{-1}), all averaged between 71 and 72 h of simulation. Contours are at 0, ± 0.5, 5, 10, 15, 20, 30, 40, 50, 60, and 70×10^{-4} s^{-1}, and regions with values greater than 5×10^{-4} s^{-1} are heavily shaded and regions with values less than $0.5 \times f_0$ are lightly shaded in (a). Contour interval is 0.5×10^6 m^2 s^{-1} in (b). Contours are at 0.5, 1, 10, 100, 500, 1000, and 5000×10^{-8} s^{-2}, and regions with values larger than 1×10^{-8} s^{-2} (100×10^{-8} s^{-2}) are lightly (heavily) shaded in (c). Contour interval is 1 m s^{-1}, and regions with values greater than 2 m s^{-1} (less than -2 m s^{-1}) are heavily (lightly) shaded in (d).

The above results demonstrate that the SE equation can be used to examine contributions of different forcing processes to the secondary circulation in the simulated tropical cyclone. Here, three calculations using the SE equation are performed: each calculation only includes one forcing term, namely the axisymmetric diabatic heating [the last term in Eq. (5)], the axisymmetric frictional forcing [the last term in Eq. (6)], or the eddy terms associated with the azimuthal-mean eddy radial and vertical fluxes of asymmetric angular momentum or the asymmetric potential temperature [the first two terms in Eqs. (5) and (6)]. Results from these calculations (Fig. 6) indicate that the secondary circulation in the middle–lower troposphere above the boundary layer is mainly a balanced

response to the axisymmetric diabatic heating, consistent with previous studies (Möller and Shapiro 2002; Bui et al. 2009). The shallow outflow immediately above the inflow boundary layer is forced mainly by the frictional forcing.

Contributions to the secondary circulation by the azimuthal-mean diabatic heating in different regions in the storm can be examined using the SE equation as well. Based on the radar reflectivity in Figs. 2c,d and the azimuthal-mean diabatic heating rate in Fig. 7a, we simply divide the azimuthal-mean diabatic heating rate into the heating rates in the eyewall within a radius of about 30 km, in inner rainbands between radii of about 30 and 70 km, and in outer rainbands and the mid–upper-tropospheric anvil clouds beyond 70 km (Figs. 7b–d,
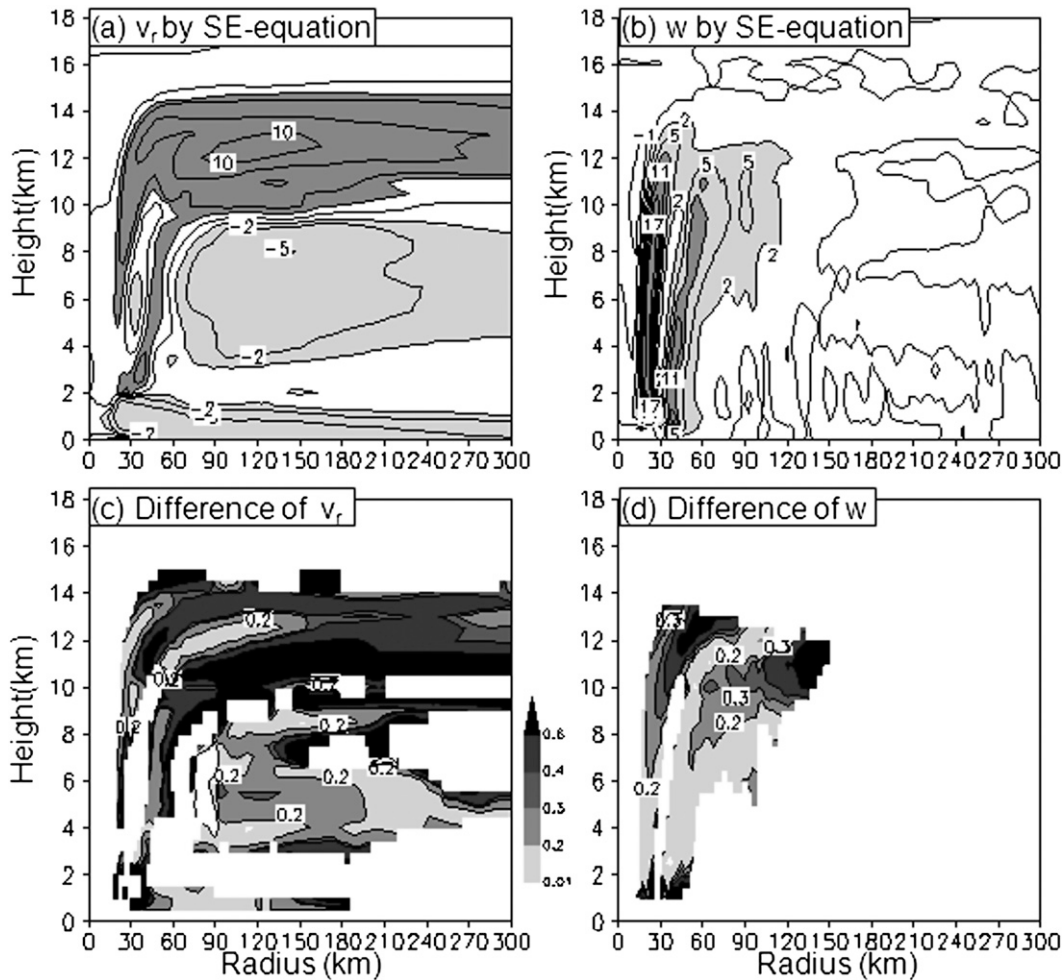
FIG. 5. The azimuthal-mean (a) radial wind (m s^{-1}) and (b) vertical velocity (10^{-1} m s^{-1}) derived from the SE equation, (c) the normalized difference D in radial wind, and (d) the normalized difference D in vertical velocity, all averaged between 71 and 72 h of simulation, as in Figs. 3a,b. Regions with D values greater than 0.01 are shaded in (c) and (d).

respectively). Figure 8 shows the secondary circulation in response to each heating source. In response to the narrow eyewall heating are a weak subsidence in the eye and an in–up–out circulation, namely a boundary layer inflow, strong eyewall updraft, an upper-tropospheric outflow, and a weak midtropospheric inflow just outside the eyewall (Figs. 8a,b), very similar to that shown in previous studies with specified eyewall-like heating (Shapiro and Willoughby 1982; Pendergrass and Willoughby 2009).

The response of the secondary circulation to heating in inner rainbands is very similar to that in the eyewall, except for the midtropospheric inflow (Figs. 8c,d). Although the azimuthal-mean diabatic heating rate in inner rainbands is only about 50% of diabatic heating in the eyewall (Figs. 7b,c), the midtropospheric inflow extends farther radially outward to beyond 200 km from the storm center (Fig. 8c). Diabatic heating in inner rainbands shows two

peaks in the vertical: one in the upper troposphere and one in the middle troposphere (Fig. 7c). Additional calculation with heating either below or above 6-km height indicates that heating in the middle–upper troposphere contributes much more to that in the midtropospheric inflow than heating in the middle–lower troposphere (not shown). The heating rate in outer rainbands and in the upper-tropospheric outflow layer between the radii of 70 and 150 km is generally less than 20% of that in the eyewall and is dominated by heating in the anvil clouds (Figs. 7b,d). It forces an inflow in the middle troposphere and an outflow in the upper troposphere in the outer-core region with quite weak azimuthal-mean vertical motion (Figs. 8e,f). The results thus suggest that the midtropospheric inflow in the outer-core region is mainly induced by mid–upper-tropospheric heating in both inner and outer rainbands.
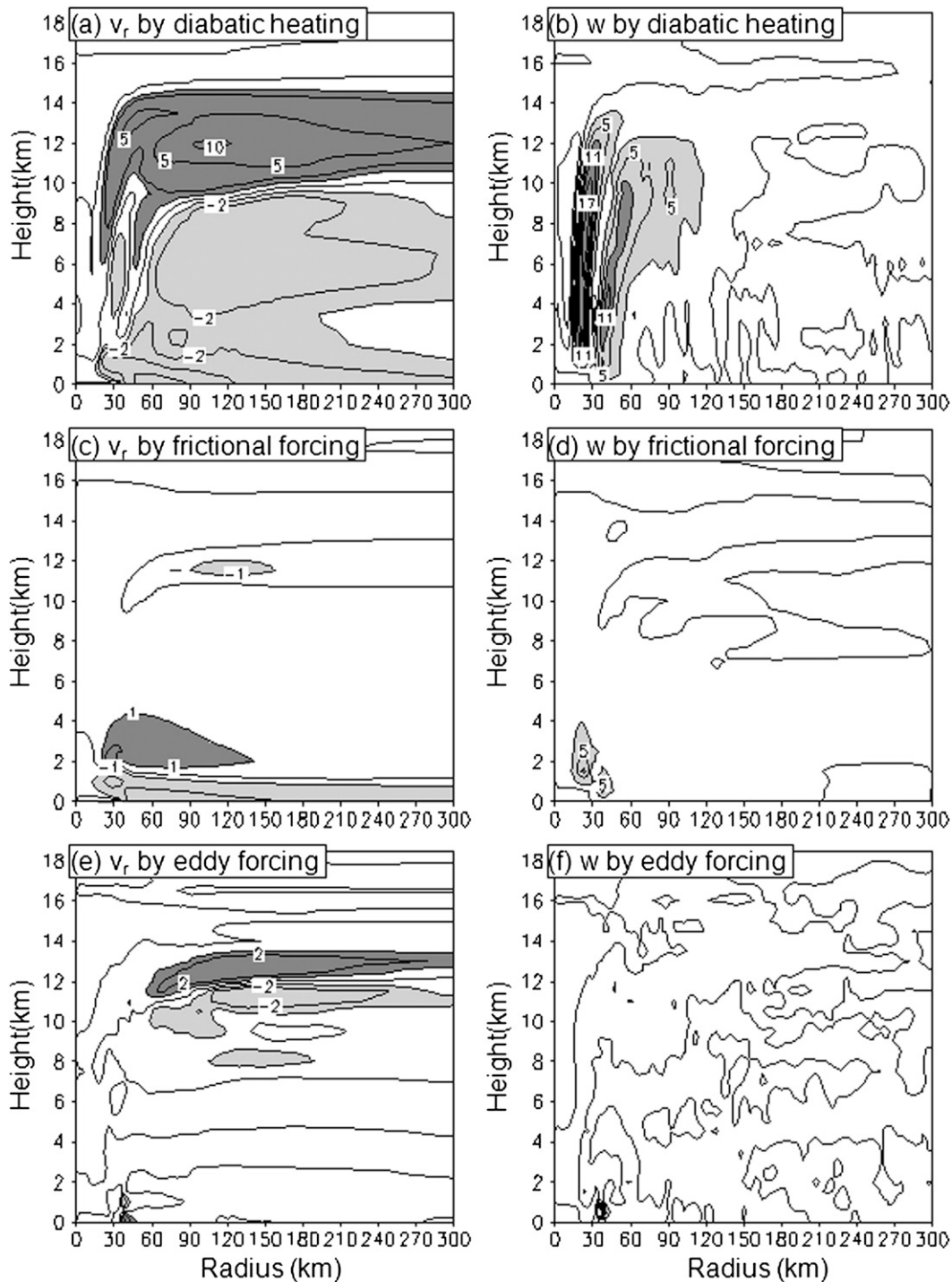
FIG. 6. (left) The azimuthal-mean radial wind (m s^{-1}) and (right) the vertical velocity (10^{-1} m s^{-1}) derived from the SE equation with the azimuthal-mean (a),(b) diabatic heating forcing; (c),(d) frictional forcing; and (e),(f) eddy heating and momentum forcing, all averaged between 71 and 72 h of simulation, as in Figs. 3a,b.
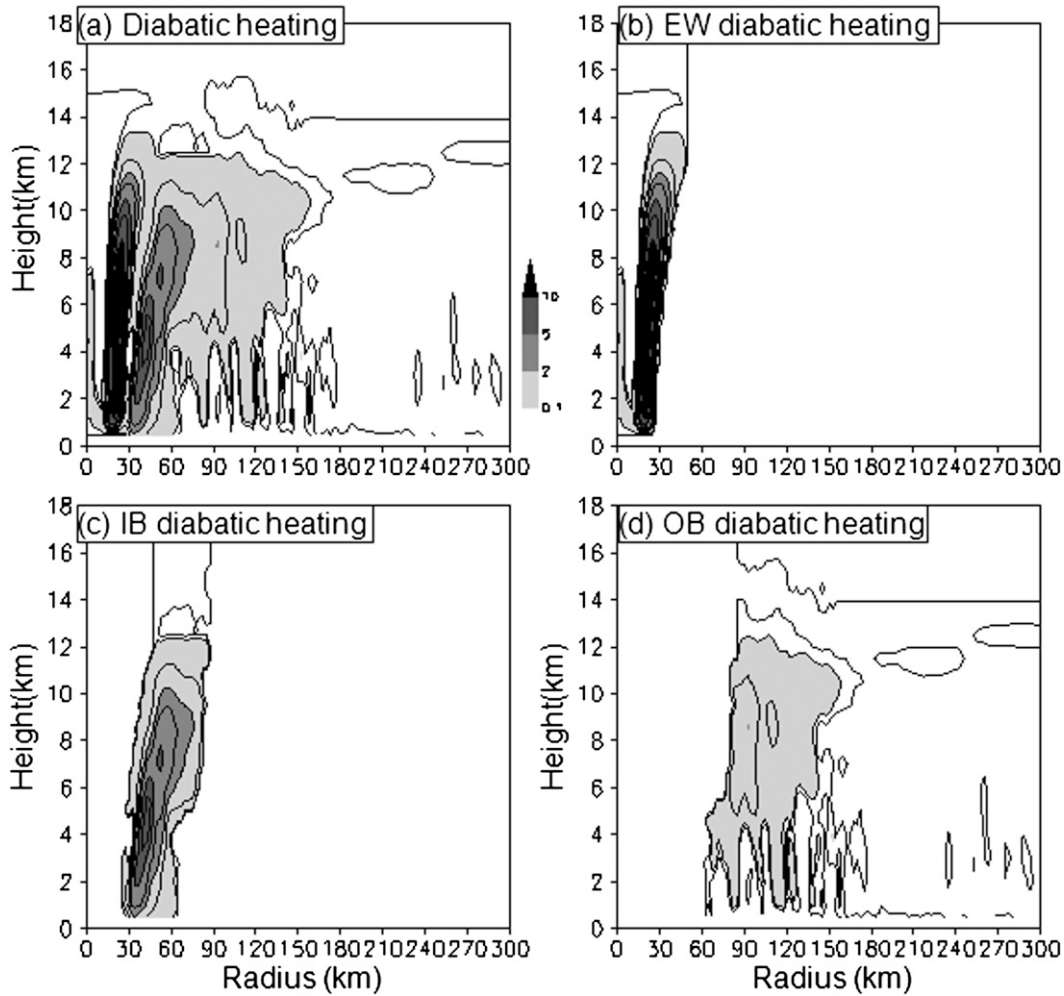
FIG. 7. The azimuthal-mean diabatic heating rate (10^{-3} K s^{-1}) of (a) total; (b) in the EW; (c) in IB; and (d) in OB and the mid–upper-tropospheric anvil clouds, all averaged between 71 and 72 h of simulation. Contours are at 0 (thick), 0.1, 1, 2, 3, 5, 7, and 10×10^{-3} K s^{-1}, and regions with values greater than 0.1×10^{-3} K s^{-1} are shaded.

4. Contributions to the spinup of outer-core circulation

To quantify the contribution by balance dynamics to the spinup of the primary circulation in the outer-core region of the simulated storm, we calculated the individual terms contributing to the azimuthal-mean tangential wind tendency. The tangential wind tendency equation in cylindrical coordinates following the moving storm can be written as (Xu and Wang 2010a,b)

$$\frac{\partial \overline{v}_t}{\partial t} = -\overline{v}_r \overline{\eta} - \overline{v'_r \eta'} - \overline{w}\frac{\partial \overline{v}_t}{\partial z} - \overline{w'\frac{\partial v'_t}{\partial z}} + \overline{F}_{sg}, \qquad (7)$$

where t is time and z is physical height. The five terms on the right-hand side are radial advection of the azimuthal-mean absolute angular momentum by the azimuthal-mean radial wind (mean radial advection), radial advection by eddy processes (eddy radial advection), vertical advection of azimuthal-mean tangential wind by the azimuthal-mean vertical motion (mean vertical advection), vertical advection by eddy processes (eddy vertical advection), and surface friction and subgrid-scale vertical mixing (friction and vertical mixing), respectively. To be consistent with discussions in the previous section, the analysis results are displayed in r–Z coordinates.

Figure 9 shows the analysis results averaged between 71 and 72 h of simulation, the same period as discussed in section 3. The time tendency of azimuthal-mean tangential wind estimated from the tangential wind tendency equation [Eq. (7); Fig. 9b] shows a distribution very similar to that simulated in TCM4 (Fig. 9a), although the former looks noisy because of the large variability of contributions by eddy processes (Fig. 9e). The difference
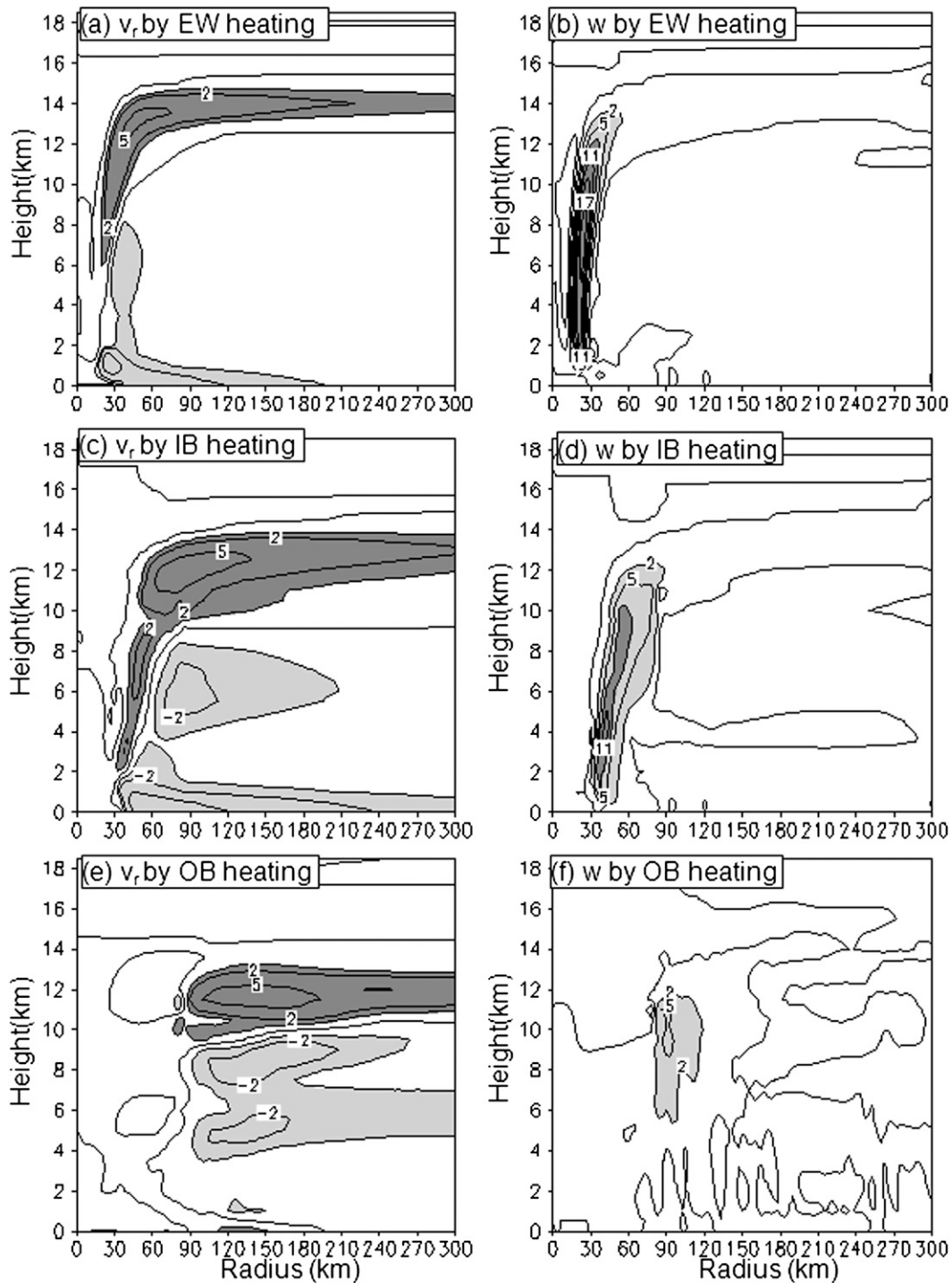
FIG. 8. (left) The azimuthal-mean radial wind (m s^{-1}) and (right) the vertical velocity (10^{-1} m s^{-1}) derived from the SE equation with the azimuthal-mean diabatic heating sources in (a),(b) the EW (Fig. 7b); (c),(d) the IB (Fig. 7c); and (e),(f) the OB and the mid–upper-tropospheric anvil clouds (Fig. 7d), all averaged between 71 and 72 h of simulation, as in Figs. 3a,b.
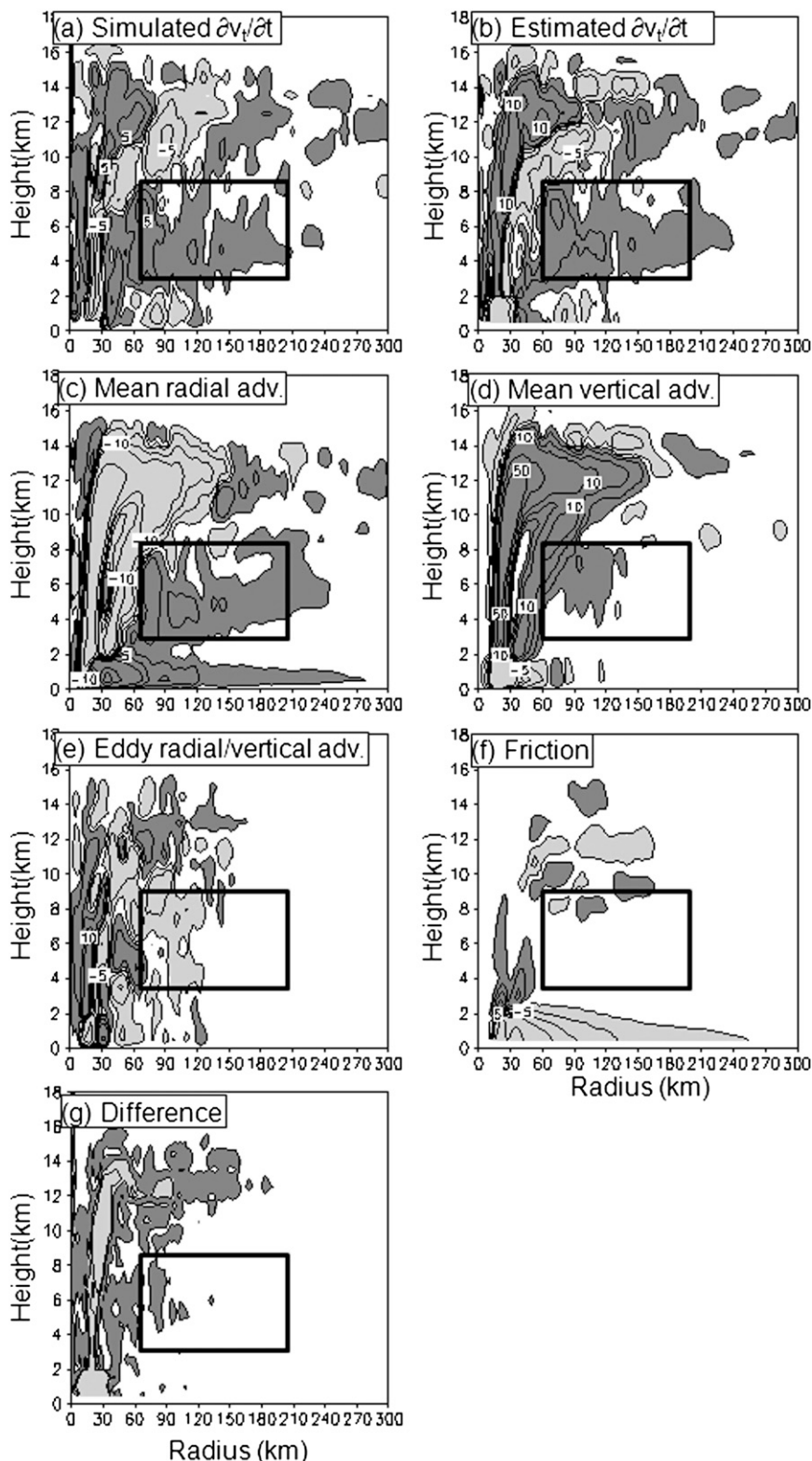
FIG. 9. The time tendency in the azimuthal-mean tangential wind (10^{-4} m s^{-2}) derived from (a) TCM4, (b) the sum of all terms in the tangential wind tendency equation, (c) mean radial advection, (d) mean vertical advection, (e) eddy radial and vertical advections, (f) friction, and (g) the difference in the tendency derived from TCM4 and from the tangential wind tendency equation, all averaged between 71 and 72 h of simulation. Contours are at ±0.5, ±2, ±5, ±10, ±30, and $\pm50 \times 10^{-4}$ m s^{-2}, and regions with values greater than 0.5×10^{-4} m s^{-2} (less than -0.5×10^{-4} m s^{-2}) are heavily (lightly) shaded in (a)–(f). Regions with values greater than 1×10^{-4} m s^{-2} (4×10^{-4} m s^{-2}) are heavily (lightly) shaded in (g). Solid box indicates the midtropospheric outer-core region.
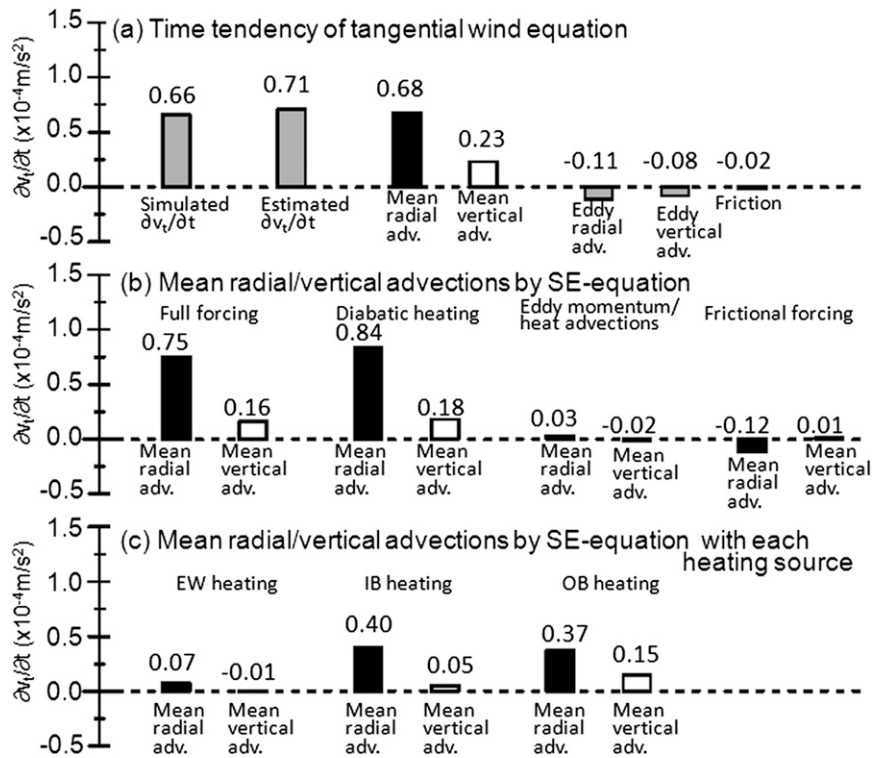
FIG. 10. Contributions to the time tendency in the azimuthal-mean tangential wind (10^{-4} m s^{-2}) by terms in the tangential wind tendency equation, averaged in a volume the midtropospheric outer-core region (the boxed area in the annulus shown in Fig. 9) and between 71 and 72 h of simulation. (a) All terms are derived from TCM4. Mean radial and vertical advections derived from the diagnosed winds by the SE equation (b) with full forcing, diabatic heating, eddy advection, and frictional forcing and (c) with diabatic heating in the EW, IB, and OB and mid–upper-tropospheric anvil clouds. Filled boxes indicate the mean radial advection, open boxes indicate the mean vertical advection, and gray boxes indicate other terms in the tangential wind tendency equation.

between the time tendency of the simulated and estimated azimuthal-mean tangential winds is small (less than 1×10^{-4} m s^{-2}) in the outer-core region throughout the troposphere and is large (greater than 4×10^{-4} m s^{-2}) in the eyewall region (Fig. 9g). Significant positive tendencies appear in the upper part in the eyewall and outside the eyewall in the middle troposphere, whereas weak negative tendencies occur in the middle–lower part in the eyewall and in the upper part of the outwardly tilted inner rainbands.

Changes in the azimuthal-mean tangential wind above the boundary layer in the eyewall and inner rainbands result mainly from the upward and outward advection of the azimuthal-mean tangential wind by the azimuthal-mean secondary circulation (Figs. 9c,d). Surface friction and vertical mixing contribute to the spindown of tangential wind in the boundary layer (Fig. 9f). Note that surface friction has an indirect effect in spinning up the wind by allowing air parcels to have larger inward radial displacements (Smith et al. 2009). Eddy processes

contribute to the spinup of tangential wind inside the eyewall and the overall spindown of tangential wind outside the eyewall in the middle–lower troposphere (Fig. 9e). The mean radial advection contributes to the spinup of tangential wind in the midtropospheric outer-core region (the boxed region in Fig. 9) with a small positive contribution by the mean vertical advection and a small negative contribution by the eddy processes. To quantify contributions to the azimuthal-mean tangential wind tendency in the midtropospheric outer-core region, in Fig. 10a we show tendencies on the right-hand side of the azimuthal-mean tangential wind tendency equation [Eq. (7)], averaged in a volume in the midtropospheric outer-core region (the boxed area in the annulus in Fig. 9). The simulated and estimated tendencies agree quantitatively well (0.66×10^{-4} versus 0.71×10^{-4} m s^{-2}). The maximum contribution to the spinup of tangential wind is by the mean radial advection (96% of estimated tendency), and the second contribution is by the mean vertical advection (32%). The eddy processes contribute negatively (total
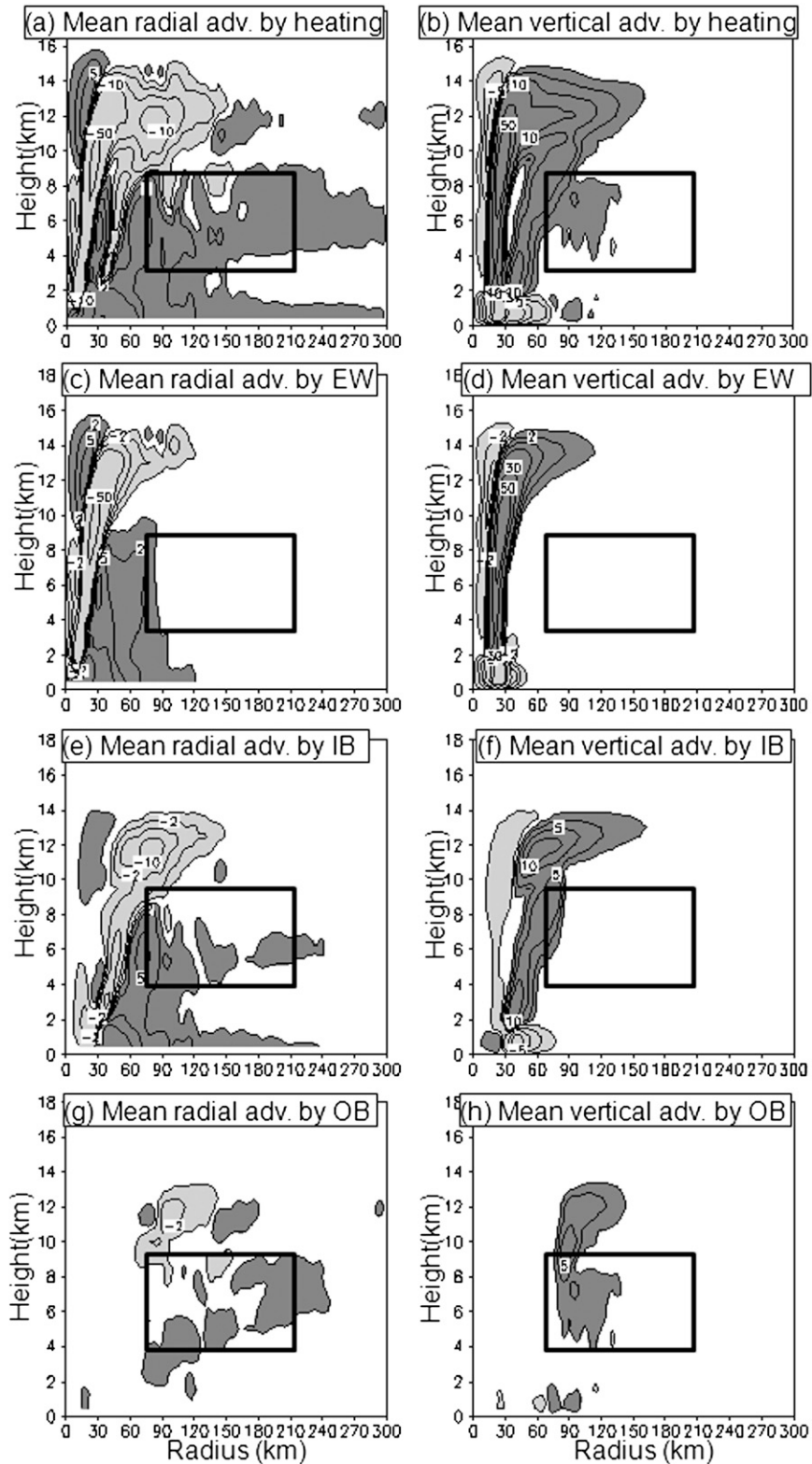
FIG. 11. As in Figs. 9c,d, but for the time tendency in the azimuthal-mean tangential wind (10^{-4} m s^{-2}) resulting from (left) the mean radial advection and (right) the mean vertical advection derived from the diagnosed winds by the SE equation with the azimuthal-mean diabatic heating in (a),(b) total; (c),(d) the EW; (e),(f) the IB; and (g),(h) the OB and mid–upper-tropospheric anvil clouds.
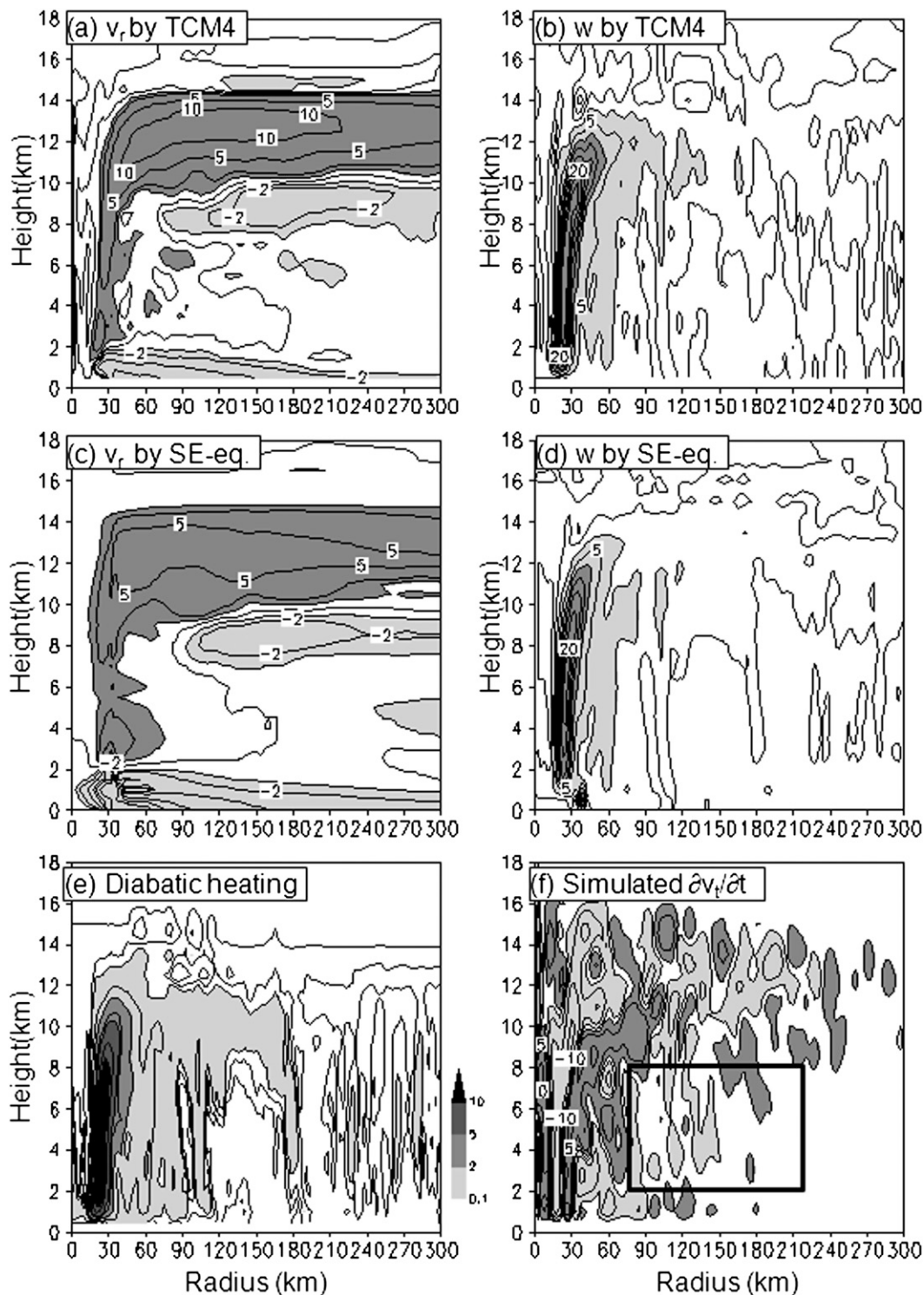
FIG. 12. The azimuthal-mean (a),(c) radial wind (m s^{-1}) and (b),(d) vertical velocity (10^{-1} m s^{-1}) derived from (a),(b) TCM4 and (c),(d) the SE equation, (e) diabatic heating rate (10^{-3} K s^{-1}), and (f) time tendency in the azimuthal-mean tangential wind (10^{-4} m s^{-2}) derived from TCM4, all averaged between 79 and 80 h of simulation. Contours are at 0 (thick), ±1, ±2, ±5, ±10, and ±15 m s^{-1}, and regions with values greater than 1 m s^{-1} (less than -1 m s^{-1}) are heavily (lightly) shaded in (a),(c). Contours are at 0 (thick), ±2, ±5, ±8, ±11, ±14, ±17, ±20, and $\pm23 \times 10^{-1}$ m s^{-1}, and regions with values greater than 2×10^{-1} m s^{-1} (8×10^{-1} m s^{-1}) are lightly (heavily) shaded in (b),(d). Contours are at 0 (thick), ±0.1, 1, 2, 3, 5, 7, and 10×10^{-3} K s^{-1}, and regions with values greater than 0.1×10^{-3} K s^{-1} are shaded in (e). Contours are at ±0.5, ±2, ±5, ±10, ±30, and $\pm50 \times 10^{-4}$ m s^{-2}, and regions with values greater than 0.5×10^{-4} m s^{-2} (less than -0.5×10^{-4} m s^{-2}) are heavily (lightly) shaded in (f).
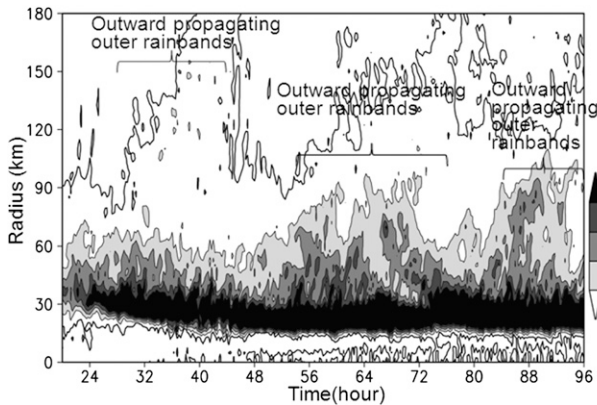
FIG. 13. Time–radius cross section of the azimuthal-mean diabatic heating rate (K s^{-1}) averaged between 3- and 12-km heights. Contours are at 0 (thick), 1, 2, 3, and 4×10^{-3} K s^{-1}, and regions with values greater than 1×10^{-3} K s^{-1} are shaded.

of -26%), whereas contribution by surface friction and vertical mixing is negligible (-2%).

Because the midtropospheric outer-core region can be well explained by balance dynamics (Fig. 5), we estimated contributions by the total and the individual heating sources to the mean radial and vertical advections of azimuthal-mean tangential wind based on the diagnosed secondary circulation from the SE equation (Figs. 10b,c). The mean radial and vertical advections of azimuthal-mean tangential wind based on SE equation solution with all forcing processes are very close to the budget directly from TCM4 output (Fig. 10a), except for a slight overestimate for the mean radial advection (0.68×10^{-4} versus 0.75×10^{-4} m s^{-2}) and an slight underestimate for the mean vertical advection (0.23×10^{-4} versus 0.16×10^{-4} m s^{-2}). Consistent with the balanced contribution to the secondary circulation as discussed in section 3 (Fig. 6), contribution by the azimuthal-mean diabatic heating to the mean radial and vertical advections of azimuthal-mean tangential wind is the largest (Fig. 10b). Contribution by the azimuthal-mean frictional forcing to the tangential wind tendency is small and negative because of the outflow just above the inflow boundary layer forced by frictional forcing (Fig. 6c), whereas contribution by the eddy processes is negligible (Figs. 6e,f). Diabatic heating in the eyewall contributes little to the spinup of tangential wind in the midtropospheric outer-core region (Figs. 10c, 11), whereas heating in both inner and outer rainbands contributes largely, consistent with the response of the secondary circulation to heating in different regions discussed in section 3. Note that the mean vertical advection, the second largest contribution to the tangential wind tendency, is mostly forced by diabatic heating in outer rainbands. Therefore, the intensification of the azimuthal-mean tangential winds in the midtropospheric

outer-core region results mostly from the mid–upper-tropospheric diabatic heating in both inner and outer rainbands.

Immediately after the active period of rainbands between 71 and 72 h of simulation as discussed above, an inactive period appears between 79 and 80 h (see Fig. 13). During this period, the azimuthal-mean diabatic heating rate is characterized by heating in the eyewall between radii of 20 and 30 km and heating in the outer rainbands around 180-km radius is dominated by mid–upper-tropospheric anvil clouds (Fig. 12e). The mean radial/vertical winds diagnosed from the SE equation (Figs. 12c,d) are qualitatively consistent with those simulated in TCM4 (Figs. 12a,b). Weak inflow appears near the 8-km height below the upper-tropospheric heating region, whereas weak outflow immediately above the inflow boundary layer extends outward from the inner-core region. As a result, the spinup of the azimuthal-mean tangential wind in the midtropospheric outer-core region (Fig. 12f) is much smaller than that between 71 and 72 h (Fig. 9a).

Figure 13 shows the time–radius cross section of the azimuthal-mean diabatic heating rate averaged between 3- and 12-km heights, and Fig. 14f shows the time evolution of the diabatic heating rate averaged between radii of 0 and 30, 30 and 70, and 70 and 150 km, respectively. The eyewall is featured by high heating rate after its contraction in the first 36 h. Diabatic heating between radii of 30 and 70 km shows some temporal variations, indicating the quasi-periodic development of inner rainbands in the simulated storm (not shown). Three episodes of the elevated diabatic heating rate initiated at about a 70-km radius during 30–44, 54–74, and 82–96 h correspond to three outward-propagating outer rainbands that appeared outside about a 70-km radius (Fig. 13) and the outward expansions in the azimuthal-mean tangential wind (Fig. 1). The azimuthal-mean diabatic heating rate associated with outer rainbands and mid–upper-tropospheric anvil clouds between radii of 70 and 150 km is much smaller than that either in the eyewall or in inner rainbands.

Figures 14a–e show the evolution of the tangential wind tendency in the midtropospheric outer-core region and contributions by mean radial, vertical, and eddy advections in the tangential wind tendency equation [Eq. (7)]. The evolution of the tangential wind tendency estimated from the tangential wind tendency equation [Eq. (7), Fig. 14b] is quantitatively very close to that directly obtained from TCM4 output (Fig. 14a). The variability in the mean radial advection mainly contributes the evolution of the azimuthal-mean tangential wind tendency (Fig. 14c), whose evolution is related to the three episodes of outward-propagating outer rainbands during 30–44, 54–74, and 82–96 h (Fig. 13). Accompanied with the three episodes are positive in the mean vertical advection
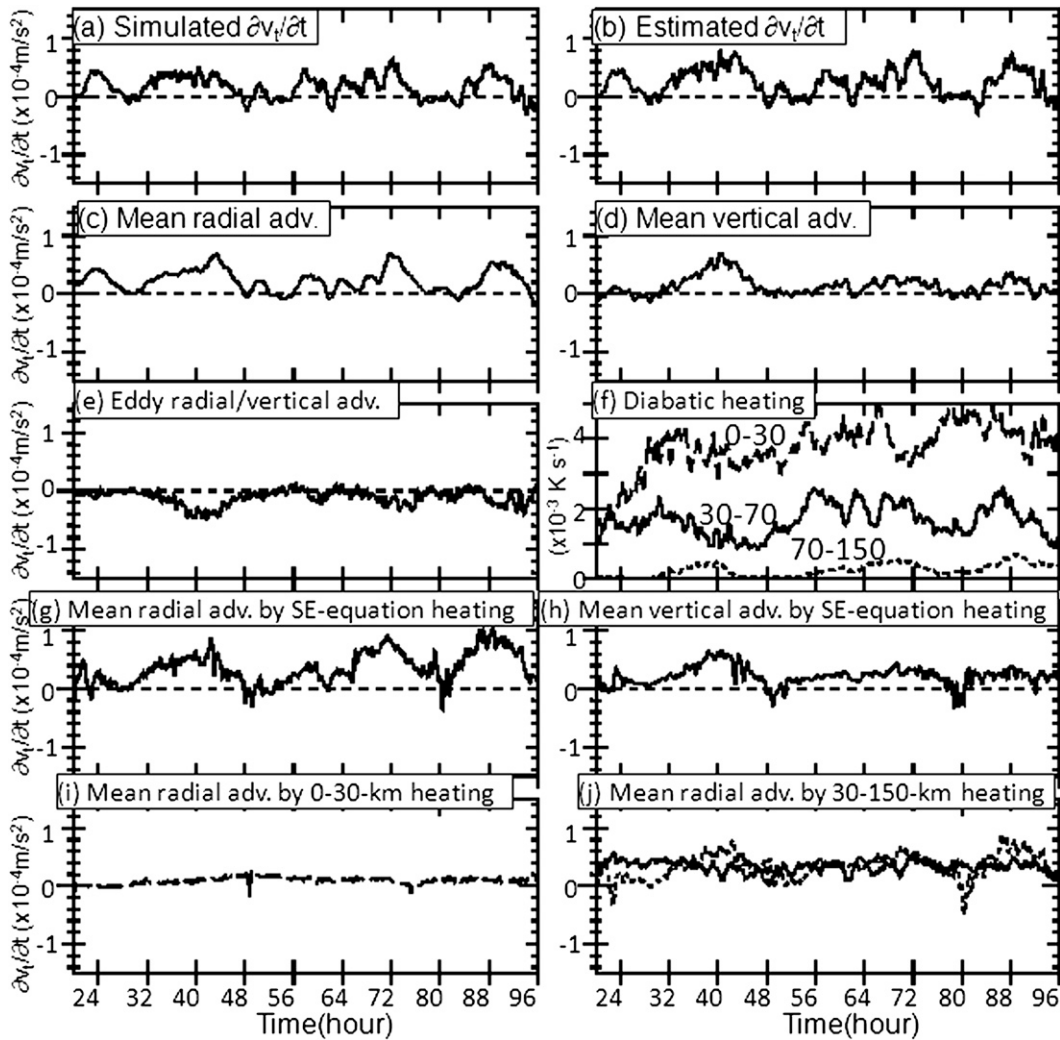
FIG. 14. Temporal evolutions of (a)–(e), (g)–(j) time tendency of the azimuthal-mean tangential wind (10^{-4} m s^{-2}) in the midtropospheric outer-core region (radii of 70–210 km and heights of 3–9 km, the box shown in Fig. 9) and (f) the azimuthal-mean diabatic heating (10^{-3} K s^{-1}) averaged between 3- and 12-km heights and between radii of 0 and 30 (dashed), 30 and 70 (solid), and 70 and 150 (dotted) km, respectively. The evolutions derived from (a) TCM4; (b) the sum of all terms in the tangential wind tendency equation; (c) mean radial advection; (d) mean vertical advection; (e) eddy radial and vertical advections; and (g),(i),(j) mean radial advection and (h) mean vertical advection based on the diagnosed winds by the SE equation with (g),(h) total diabatic heating and (i),(j) diabatic heating between (i) radii of 0 and 30 km (dashed) and (j) between radii of 30 and 70 (solid) and 70 and 150 km (dotted), respectively.

associated with the activity of outer rainbands (Fig. 14d). Overall, the eddy associated with outer rainbands spins down the midtropospheric outer-core circulation, partly offsetting the spinup by the mean radial/vertical advections (Fig. 14e). Therefore, three processes associated with outer rainbands may contribute to the spinup of the midtropospheric outer-core region: overall positive contributions by the mean radial and vertical advections and a negative contribution by eddy advections.

Figures 14g–j show the mean radial and vertical advections based on the diagnosed secondary circulation

derived from the SE equation. The evolution of the mean radial and vertical advections obtained from the SE equation with total diabatic heating (Figs. 14g,h) is quantitatively very close to that estimated from the tangential wind tendency equation [Eq. (7), Figs. 14c,d]. Diabatic heating between radii of 30 and 70 km and between radii of 70 and 150 km in both inner and outer rainbands contributes the evolution of the mean radial advection (Figs. 14i,j), whereas the evolution of the mean vertical advection is consistent with the evolution of diabatic heating between radii of 70 and 150 km in outer
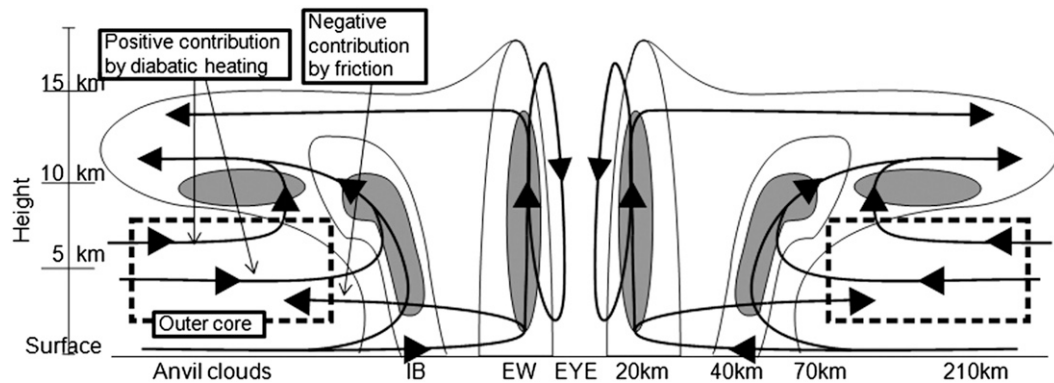
FIG. 15. Schematic diagram showing the azimuthal-mean secondary circulation forced by the azimuthal-mean diabatic heating in the EW, IB, and mid–upper-tropospheric anvil clouds and surface friction. Regions with significant diabatic heating are shaded. Arrows indicate azimuthal-mean secondary circulation. Dashed boxes indicate the region of the midtropospheric outer-core region. The outer-core spinup process is associated with the midtropospheric inflow in response to the mid–upper-tropospheric diabatic heating outside the eyewall.

rainbands (not shown). These further demonstrate that diabatic heating in both inner and outer rainbands is important for the spinup of the midtropospheric circulation in the outer-core region.

5. Conclusions and discussion

a. Conclusions

We have examined contributions by diabatic heating in different regions to the spinup of the outer-core circulation in a tropical cyclone simulated in the three-dimensional, nonhydrostatic, full-physics model TCM4 by solving the SE equation and by computing terms in the azimuthal-mean tangential wind tendency equation. The azimuthal-mean secondary circulation (radial and vertical circulation) and the spinup of the midtropospheric outer-core circulation in the simulated tropical cyclone are well captured by the SE equation, namely by balance dynamics. The azimuthal-mean tangential wind tendency equation shows that the mean radial and vertical advections that are mainly driven by diabatic heating in spiral rainbands and in the upper-tropospheric anvil clouds outside the eyewall contributed the spinup of the primary circulation in the midtropospheric outer-core region immediately outside the inner core.

Figure 15 provides a synthesis of the outer-core spinup process based on our diagnostic analyses. The azimuthal-mean diabatic heating outside the eyewall in the middle–upper troposphere drives radial inflow in the outer-core region in the middle troposphere. The radial inflow brings about high absolute angular momentum inward to intensify the primary circulation in the midtropospheric outer-core region. Although the diabatic heating rate in

the eyewall is the largest, its contribution to the spinup of the midtropospheric outer-core primary circulation is generally much less than diabatic heating outside the eyewall because of the high inertial stability in the inner-core region. Diabatic heating in outer rainbands contributes positively to the spinup of the outer-core primary circulation by the mean vertical and radial transport of angular momentum and negatively by the eddy advections. The contribution by surface friction to the tangential wind tendency is negligible above the inflow boundary layer, whereas the outflow just above the inflow boundary layer in response to surface friction contributes negatively to the outer-core primary circulation above the boundary layer.

b. Discussion

This study demonstrates the important contribution of diabatic heating outside the eyewall to the secondary circulation and the spinup of the outer-core primary circulation of a simulated tropical cyclone. Recently, Smith et al. (2009) and Bui et al. (2009) showed that the increase in the outer-core circulation above the inflow boundary layer results from the radial convergence of the absolute angular momentum. We have extended their work to examine the contributions of diabatic heating in different regions in the storm to the spinup of the outer-core circulation. We show that diabatic heating in both inner and outer rainbands, in particular that in the mid–upper-tropospheric anvil clouds, plays a dominant role.

Weatherford and Gray (1988a,b) showed the independency between the inner-core intensity (storm intensity) and the outer-core strength (winds outside the eyewall). Our azimuthal-mean tangential wind tendency equation

shows that the inner-core strength can be explained by the mean vertical advection of azimuthal-mean tangential wind above the boundary layer and radial advection of azimuthal-mean tangential wind within the boundary layer (Fig. 9). Diabatic heating in the eyewall contributes to the inner-core strength and thus the storm intensity. Diabatic heating in the middle–upper troposphere in both inner and outer rainbands contributes largely to the spinup of the outer-core strength, whereas it contributes little to the inner-core strength or storm intensity (Fig. 15).

Wang (2009) evaluated the effect of diabatic heating in outer spiral rainbands on the storm structure and intensity through sensitivity experiments by artificially modifying the heating rate in the region outside a radius of about 90 km. He found that diabatic heating in outer rainbands limits the storm intensity while it increases the storm inner-core size. In this study, we have further quantified the spinup process of the outer-core circulation by heating in outer rainbands based on balance dynamics. The results confirm that diabatic heating outside the eyewall (both in inner and outer spiral rainbands) contributes predominantly to the spinup of the outer-core circulation and thus the increase in storm-scale size. Our finding also supports the results of Hill and Lackmann (2009), who showed that the tropical cyclone size in their cloud-resolving simulation was sensitive to the environmental relative humidity. In a relatively moist environment, the storm developed considerable precipitation (and thus diabatic heating) outside the core (in spiral rainbands), accompanied by significant outward expansion of the wind field and increase in storm size.

We also demonstrated that balance dynamics can capture the detailed features of the secondary circulation simulated in a full-physics model, including its temporal evolution. Therefore, balance dynamics can be applied to the understanding of structure and intensity changes of the tropical cyclone simulated in high-resolution nonhydrostatic models as a diagnostic tool, consistent with the conclusions of Bui et al. (2009). In particular, balance dynamics can help estimate potential contributions of a heating source in different radial range and different vertical layers to the intensification and size change of the simulated tropical cyclone. This study is a first step toward the understanding of the spinup process of the outer-core circulation in a tropical cyclone simulated in a full-physics model under idealized conditions based on balance dynamics. The findings are valid only for a quasi-axisymmetric storm, because the simulation was performed on an f plane in a quiescent environment. With any environmental forcing, the storm may develop considerable asymmetric structure. In that case, the eddy processes enhanced by the environmental forcing may have considerable contribution to the spinup of the outer-core circulation. In addition, the outer-core strength and storm size should be significantly affected by environmental synoptic conditions, which may influence activity of spiral rainbands and modify the distribution of diabatic heating in the tropical cyclone circulation (Merrill 1984; Holland and Merrill 1984; Weatherford and Gray 1988b; Cocks and Gray 2002). We plan to include the effect of environmental flow in a future study.

REFERENCES

Barnes, G. M., E. J. Zipser, D. Jorgensen, and F. Marks, 1983: Mesoscale and convective structure of a hurricane rainband. *J. Atmos. Sci.,* **40,** 2125–2137.

Bui, H. H., R. K. Smith, M. T. Montgomery, and J. Y. Peng, 2009: Balanced and unbalanced aspects of tropical cyclone intensification. *Quart. J. Roy. Meteor. Soc.,* **135,** 1715–1731.

Cocks, S. B., and W. M. Gray, 2002: Variability of the outer wind profiles of western North Pacific typhoons: Classifications and techniques for analysis and forecasting. *Mon. Wea. Rev.,* **130,** 1989–2005.

Eliassen, A., 1952: Slow thermally or frictionally controlled meridional circulation in a circular vortex. *Astrophys. Norv.,* **5,** 19–60.

Fairall, C. W., E. F. Bradley, J. E. Hare, A. A. Grachev, and J. B. Edson, 2003: Bulk parameterization of air–sea fluxes: Updates and verification for the COARE algorithm. *J. Climate,* **16,** 571–591.

Fudeyasu, H., Y. Wang, M. Satoh, T. Nasuno, H. Miura, and W. Yanase, 2010: Multiscale interactions in the lifecycle of a tropical cyclone simulated in a global cloud-system-resolving model: Part II: System-scale and mesoscale processes. *Mon. Wea. Rev.,* **138,** 4305–4327.

Gray, W. M., E. Ruprecht, and R. Phelps, 1975: Relative humidity in tropical weather systems. *Mon. Wea. Rev.,* **103,** 685–690.

Hack, J. J., and W. H. Schubert, 1986: Nonlinear response of atmospheric vortices to heating by organized cumulus convection. *J. Atmos. Sci.,* **43,** 1559–1573.

Hendricks, E. A., M. T. Montgomery, and C. A. Davis, 2004: The role of ''vortical'' hot towers in the formation of Tropical Cyclone Diana (1984). *J. Atmos. Sci.,* **61,** 1209–1232.

Hill, K. A., and G. M. Lackmann, 2009: Influence of environmental humidity on tropical cyclone size. *Mon. Wea. Rev.,* **137,** 3294–3315.

Holland, G. J., and R. T. Merrill, 1984: On the dynamics of tropical cyclone structural changes. *Quart. J. Roy. Meteor. Soc.,* **110,** 723–745.

Kepert, J., and Y. Wang, 2001: The dynamics of boundary layer jets within the tropical cyclone core. Part II: Nonlinear enhancement. *J. Atmos. Sci.,* **58,** 2485–2501.

Langland, R. H., and C.-S. Liou, 1996: Implementation of an E–ε parameterization of vertical subgrid-scale mixing in a regional model. *Mon. Wea. Rev.,* **124,** 905–918.

Marks, F. D., and R. A. Houze, 1987: Inner core structure of Hurricane Alicia from airborne Doppler radar observations. *J. Atmos. Sci.,* **44,** 1296–1317.

——, P. G. Black, M. T. Montgomery, and R. W. Burpee, 2008: Structure of the eye and eyewall of Hurricane Hugo (1989). *Mon. Wea. Rev.,* **136,** 1237–1259.

Merrill, R. T., 1984: A comparison of large and small tropical cyclones. *Mon. Wea. Rev.,* **112,** 1408–1418.

Molinari, J., and D. Vollaro, 1990: External influences on hurricane intensity. 2. Vertical structure and response of the hurricane vortex. *J. Atmos. Sci.,* **47,** 1902–1918.

——, ——, and S. Skubis, 1993: Application of the Eliassen balanced model to real-data tropical cyclones. *Mon. Wea. Rev.,* **121,** 2409–2419.

Möller, J. D., and L. J. Shapiro, 2002: Balanced contributions to the intensification of Hurricane Opal as diagnosed from a GFDL model forecast. *Mon. Wea. Rev.,* **130,** 1866–1881.

Montgomery, M. T., M. E. Nicholls, T. A. Cram, and A. B. Saunders, 2006: A vortical hot tower route to tropical cyclogenesis. *J. Atmos. Sci.,* **63,** 355–386.

Pendergrass, A. G., and H. E. Willoughby, 2009: Diabatically induced secondary flows in tropical cyclones. Part I: Quasi-steady forcing. *Mon. Wea. Rev.,* **137,** 805–821.

Persing, J., M. T. Montgomery, and R. E. Tuleya, 2002: Environmental interactions in the GFDL hurricane model for Hurricane Opal. *Mon. Wea. Rev.,* **130,** 298–317.

Rotunno, R., and K. A. Emanuel, 1987: An air-sea interaction theory for tropical cyclones. Part II: Evolutionary study using a nonhydrostatic axisymmetric model. *J. Atmos. Sci.,* **44,** 542–561.

Schubert, W. H., and J. J. Hack, 1982: Inertial stability and tropical cyclone development. *J. Atmos. Sci.,* **39,** 1687–1697.

Shapiro, L. J., and H. E. Willoughby, 1982: The response of balanced hurricanes to local sources of heat and momentum. *J. Atmos. Sci.,* **39,** 378–394.

Smith, R. K., and M. T. Montgomery, 2008: Balanced boundary layers used in hurricane models. *Quart. J. Roy. Meteor. Soc.,* **134,** 1385–1395.

——, ——, and N. Van Sang, 2009: Tropical cyclone spin-up revisited. *Quart. J. Roy. Meteor. Soc.,* **135,** 1321–1335.

Wang, Y., 2001: An explicit simulation of tropical cyclones with a triply nested movable mesh primitive equation model: TCM3. Part I: Model description and control experiment. *Mon. Wea. Rev.,* **129,** 1370–1394.

——, 2002: An explicit simulation of tropical cyclones with a triply nested movable mesh primitive equation model: TCM3. Part II: Model refinements and sensitivity to cloud microphysics parameterization. *Mon. Wea. Rev.,* **130,** 3022–3036.

——, 2007: A multiply nested, movable mesh, fully compressible, nonhydrostatic tropical cyclone model—TCM4: Model description and development of asymmetries without explicit asymmetric forcing. *Meteor. Atmos. Phys.,* **97,** 93–116.

——, 2008a: Structure and formation of an annular hurricane simulated in a fully compressible, nonhydrostatic model—TCM4. *J. Atmos. Sci.,* **65,** 1505–1527.

——, 2008b: Rapid filamentation zone in a numerically simulated tropical cyclone. *J. Atmos. Sci.,* **65,** 1158–1181.

——, 2009: How do outer spiral rainbands affect tropical cyclone structure and intensity? *J. Atmos. Sci.,* **66,** 1250–1273.

——, and J. Xu, 2010: Energy production, frictional dissipation, and maximum intensity of a numerically simulated tropical cyclone. *J. Atmos. Sci.,* **67,** 97–116.

Weatherford, C. L., and W. M. Gray, 1988a: Typhoon structure as revealed by aircraft reconnaissance. Part I: Data analysis and climatology. *Mon. Wea. Rev.,* **116,** 1032–1043.

——, and ——, 1988b: Typhoon structure as revealed by aircraft reconnaissance. Part II: Structural variability. *Mon. Wea. Rev.,* **116,** 1044–1056.

Willoughby, H. E., 1979: Forced secondary circulations in hurricanes. *J. Geophys. Res.,* **84,** 3173–3183.

Xu, J., and Y. Wang, 2010a: Sensitivity of tropical cyclone inner-core size and intensity to the radial distribution of surface entropy flux. *J. Atmos. Sci.,* **67,** 1831–1852.

——, and ——, 2010b: Sensitivity of the simulated tropical cyclone inner-core size to the initial vortex size. *Mon. Wea. Rev.,* **138,** 4135–4157.